RSC Advances

ROYAL SOCIETY OF CHEMISTRY

www.rsc.org/advances

Journal Name

RSCPublishing

ARTICLE

Fabrication and characterization of β-PbO_2/α-PbO_2/Sb-SnO_2/TiO_2 nanotube arrays electrode and its application in electrochemical degradation of Acid Red G

Cite this: DOI: 10.1039/x0xx00000x

Received ooth January 2012,
Accepted ooth January 2012

DOI: 10.1039/x0xx00000x

www.rsc.org/

Jia Wu [a], Hao Xu [*a], Wei Yan [*a, b]

A novel β-PbO2/α-PbO2/Sb-SnO2/TiO2 nanotube arrays electrode was fabricated and investigated for the treatment of Acid Red G (ARG) in aqueous solution. Microwave method and electrodeposition method were employed for the deposition of Sb-SnO2 and PbO2 on the TiO2 nanotube arrays template, respectively. The structure and surface morphology of the composite electrode were characterized by X-ray diffraction (XRD) and field-emission scanning electron microscopy (FE-SEM). Electrochemical measurements including cyclic voltammetry (CV), electrochemical impedance spectroscopy (EIS) and accelerated life measurements were employed to investigate the electrochemical activity and stability of the hybrid electrode. The obtained composite electrode had an ordered multilayer structure with TiO2 nanotube arrays as a tubal template and Sb-SnO2 coating as an interlayer, which exhibited an enhanced electrocatalytic activity, long lifetime (815 h) and high oxygen evolution reaction potential. Acid Red G (ARG) was employed as a model organic pollutant for electrochemical degradation to evaluate the electrocatalytic activity of the composite electrode. Several operation variables, such as initial concentration, current densities, initial pH values, temperature of electrolyte, and chloride ions were investigated to explore the removal efficiency of ARG. It was found that low concentration, high current densities and addition of chloride ions could significantly improve the colour removal efficiency. Nevertheless, variables of pH and temperature had little impact on the colour removal efficiency. These results show that the hybrid electrode may become a promising electrode in treating wastewater.

1. Introduction

Electrochemical oxidation has attracted wide attentions in treating refractory or toxic wastewater recent years due to its environmental compatibility, easy automation, high efficiency and mineralization [1-5]. As we all known, the electrode material is a significant factor for effective electrochemical oxidation process [6]. Therefore, development of the electrodes with high stability and electrochemical activity have become a hotspot. A wide variety of electrode materials such as boron-doped diamond (BDD) [7-9], Pt [10-11], IrO_2 [12], RuO_2 [13], SnO_2 [14-19] and PbO_2 [20-27] have been studied. Among these electrodes, SnO_2 and PbO_2 are commonly used dimensionally-stable anodes (DSAs) for removal of organic contamination due to their high oxygen over-potential. SnO_2 has the advantage of lower cost than other noble metal oxides and is usually doped with Sb to enhance its electrical conductivity [28]. Nevertheless, the short service lifetime of SnO_2 electrodes has confined its practical application [29]. PbO_2 electrodes are cheap materials and facile to fabricate, with well electrochemical stability, high oxygen evolution potential and long service lifetime [30-34], which make PbO_2 electrodes attract much interest. Many efforts have been spent on prompting the performance of PbO_2 electrodes. New dopants implanted into PbO_2 including Co [35], Ce [36], Bi [37], Fe [38], F [39] and Cu [40] ions into PbO_2 has been discussed.

Highly ordered, vertically oriented TiO_2 nanotube arrays (NTAs) have been given much attention due to their big surface area, well hydrophilicity, high uniformity and orientation. These characteristics can make them act as remarkable template for further decorating catalysts and enhance the electrochemical activity of SnO_2 or PbO_2 electrodes [41-46]. Thermal decomposition and electrodeposition are common methods for preparation of the traditional Sb-SnO_2 coating. Some researchers claimed that a more uniform and dense coating can be obtained by the electrodeposition process [42]. However, the problem of surface tension on the TiO_2 nanotube arrays surface needs to be solved in the application of these methods. Microwave method has the advantage of high pressure and

power, which was expected to decrease the surface intension. Therefore, in this paper, interlayer of Sb-SnO_2 coating embedding into TiO_2 nanotube arrays by microwave method has been introduced into PbO_2 electrodes system with the aim to decrease surface intension and enhance electrocatalytic activity.

The principle diagram of this novel composite electrode is shown in Fig. 1. Firstly, highly ordered TiO_2 nanotube arrays in situ grown on Ti substrate was fabricated by anodic oxidation (Fig. 1a, Fig. 1b), then Sb-SnO_2 coating was implanted into TiO_2 nanotube arrays by novel microwave method (Fig. 1c), finally α-PbO_2 and β-PbO_2 were successively deposited onto the Sb-SnO_2 coating by electrodeposition method under various deposition solution, deposition temperature and deposition time (Fig. 1d, Fig. 1e). In the composite electrode, TiO_2 nanotube arrays could act as a tubal template; Sb-SnO_2 coating was employed as an interlayer to enhance the electrocatalytic activity and electrochemical stability of PbO_2 coating; α-PbO_2 coating was applied to provide better contact between the particles because of its compact structure; β-PbO_2 coating was used as a surface layer to enhance the electrocatalytic activity and service lifetime. This well-aligned multilayer structure was expected to improve the specific surface area and loading amount of the composite electrode. Therefore, this thesis proposes a novel β-PbO_2/α-PbO_2/Sb-SnO_2/TiO_2 nanotube arrays electrode combining the microwave and electrodepositon in order to increase its electrochemical performance and stability.

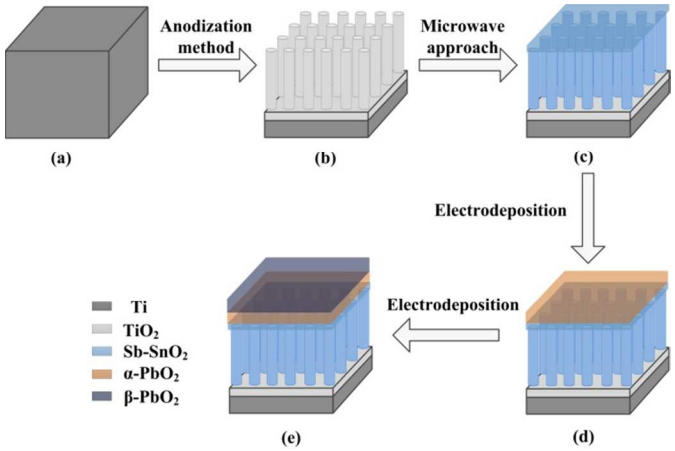

Fig. 1 The principle diagram of the β-PbO_2/α-PbO_2/Sb-SnO_2/TiO_2 nanotube arrays electrode. (a) Ti foil; (b) TiO_2 NTAs; (c) Sb-SnO_2/TiO_2 NTAs; (d) α-PbO_2/Sb-SnO_2/TiO_2 NTAs; (e) β-PbO_2/α-PbO_2/Sb-SnO_2/TiO_2 NTAs.

The aim of this work is focused on the electrocatalytic performance and stability of β-PbO_2/α-PbO_2/Sb-SnO_2/TiO_2 nanotube arrays electrode. Acid Red G (ARG) was employed as a model organic pollutant for electrochemical degradation for the purpose of evaluating its electrocatalytic activity. The colour removal efficiency of ARG was studied by UV-Vis analysis. It was discussed as a function of several experimental variables, such as initial concentration, current densities, initial pH values, temperature of electrolyte and chloride ions.

2. Experimental details

2.1 Materials

All chemicals were of analytical grade and were employed without any further purification. All aqueous solutions were prepared with deionized (DI) water. The titanium foil (>99.6% purity, BaoTi Co. Ltd, China, 0.5 mm) was cut into pieces with a dimension of 2×4.5 cm before experiments.

2.2 Synthesis of TiO_2 nanotube arrays

Highly oriented TiO_2 nanotube arrays were formed on the titanium foil by anodization method. Prior to electrochemical anodization, samples were degreased by ultrasonicating (SG5200HPT, Shanghai Guante Co. Ltd, China) in isopropanol, acetone and ethanol, followed by rinsing with DI and drying in air without any additional surface polishing. Anodization was carried out in the two-electrode configuration with the Ti sheet as both cathode and anode at room temperature. The distance between the two electrodes was 2.5 cm. Anodization was conducted for 1 h with magnetic stirring at a voltage of 50 V (JBP15005, Jiangbo Co. Ltd, China) in the ethylene glycol (EG) containing 0.3 wt% NH_4F (99.5%) and 3 vol% H_2O electrolyte. After anodization, the sample was washed thoroughly with DI and then exposed to ultrasonication (100 W, 59 kHz) to remove the sediment. These obtained TiO_2 nanotube arrays were annealed (GMF1100, Hefei Kejin Co. Ltd, China) in air at 500 ℃ for 2 h to induce crystallization, with a heating and cooling rate of 1℃/min.

2.3 Fabrication of Sb-SnO_2/TiO_2 nanotube arrays

Sb and Sn were deposited into TiO_2 nanotube arrays by microwave approach (Multiwave 3000, Anton Paar). The precursor solution of $SnCl_4{\cdot}5H_2O$ and $SbCl_3$ was freshly prepared by dissolving 0.05 M $SnCl_4{\cdot}5H_2O$ and 0.005 M $SbCl_3$ in absolute ethanol with magnetic stirring (IKA colour squid). These as-prepared TiO_2 nanotube arrays were fixed in Teflon lined microwave digestion vessel containing synthesis solution and ultrasonic immersing for 20 min (50 W, 59 kHz). Experimental parameters were set as follows: pressure of 30 bar, 600 W in power, temperature of 180℃, heating time of 15 min, retention time of 90 min and cooling time of 15 min. After reaction, these resulted Sb-SnO_2/TiO_2 nanotube arrays electrodes were washed thoroughly with ethanol and deionized water and then dried in air. Finally, obtained Sb-SnO_2/TiO_2 nanotube arrays electrodes were annealed at 500℃ for 1 h with a heating and cooling rate of 5℃/min in air atmosphere.

2.4 Deposition of PbO_2 onto Sb-SnO_2/TiO_2 nanotube arrays

In this procedure, PbO_2 coating was fabricated on Sb-SnO_2/TiO_2 nanotube arrays by electrodeposition of an inner layer (α-PbO_2) and an outer layer (β-PbO_2). The inner layer α-PbO_2 was carried out to prepare an interlayer between the Sb-SnO_2 coating and the surface β-PbO_2 layer. It is helpful for stability and contact of the entire PbO_2 coating. The deposition solution was composed of 3.5 mol·L^{-1} NaOH and 0.11 mol·L^{-1}

PbO. This procedure employed a two-electrode system, in which copper sheet was employed as cathode and Sb-SnO_2/TiO_2 nanotube arrays electrode was used as anode. This deposition process was conducted in a cylindrical reactor under a current density of 10 mA·cm^{-2} for 30 min. The deposition solution was maintained at 40℃ with constant temperature water-bathing (501A, Shanghai Co. Ltd, China) and stirred by magnetic stirring in this process. The resulted α-PbO_2/Sb-SnO_2/TiO_2 nanotube arrays electrode was washed thoroughly with DI water and dried in air. Finally, outer layer β-PbO_2 was deposited on α-PbO_2/Sb-SnO_2/TiO_2 nanotube arrays electrode with a current density of 10 mA·cm^{-2} for 120 min under 65℃ by electrodeposition. This deposition solution consisted of 0.01 mol·L^{-1} NaF, 0.2 mol·L^{-1} $Cu(NO_3)_2$ and 0.5 mol·L^{-1} $Pb(NO_3)_2$ and the pH was adjusted to 2.0 by using concentrated HNO_3. The as-prepared electrode was denoted as β-PbO_2/α-PbO_2/Sb-SnO_2/TiO_2 nanotube arrays electrode and was rinsed thoroughly with deionized water.

2.5 Characterization

Field-emission scanning electron microscopy (FE-SEM, JEOL, JSM-6700F) equipped with an energy-dispersive X-ray spectroscopy (EDS) detector was employed to investigate the surface morphology of prepared sample. X-ray diffraction (XRD) measurements were performed on an X'pert PRO MRD diffractometer using Cu-Kα source (λ=0.15416 nm), with a scanning angle (2θ) range of 10-80°.

Electrochemical performance of as-prepared β-PbO_2/α-PbO_2/Sb-SnO_2/TiO_2 nanotube arrays electrode was performed on a CHI 660D electrochemical workstation (Chenhua, Shanghai) using a traditional three-electrode system. A saturated Ag/AgCl electrode was employed as reference electrode and a Pt sheet as counter electrode. Linear sweep voltammetric (LSV) characterization was conducted in 0.5 mol·L^{-1} H_2SO_4 aqueous solutions at a scan rate of 50 mV·s^{-1}. Moreover, cyclic voltammetry (CV) measurements were also carried out in 0.5 mol·L^{-1} H_2SO_4 aqueous solutions between different potential limits at a scan rate between 10 and 100 mV·s^{-1}. Voltammetric charge (q^*) were determined by integrating the area of cyclic voltammograms.

Electrochemical impedance spectroscopy (EIS) measurements were conducted to understand the charge transport performance of the composite electrode. The frequency range used is 100 kHz to 0.01 Hz and the amplitude of sinusoidal wave is 10 mV.

Accelerated life measurements were carried out to investigate electrochemical lifetime of β-PbO_2/α-PbO_2/Sb-SnO_2/TiO_2 nanotube arrays electrode in 0.5 mol·L^{-1} H_2SO_4 aqueous solutions with a current density of 0.5 A·cm^{-2}. In this step, the experiment was supposed to be finished when the cell voltage was higher than 10 V.

2.6 Electrocatalytic degradation process

Electrocatalytic degradation experiment was carried out in a cylindrical cell equipped with a magnetic stirrer using a two-electrode system, as shown in Fig. 2. The as-prepared β-PbO_2/α-PbO_2/Sb-SnO_2/TiO_2 nanotube arrays electrode was employed as anode and copper foil was used as cathode. These dye solutions containing acid red G (ARG) were fabricated by dissolving ARG dye in 200 mL of 0.1 M Na_2SO_4. Influence of initial dye concentrations, initial pH values, current densities, temperature of electrolyte and chloride ions were investigated to discuss the degradation efficiency of the dye. Initial dye concentrations of 20, 40, 60, 80, and 100 mg·L^{-1} were employed to examine the effect of different concentrations on the colour removal efficiency of the dye. Current densities of 10, 20, 30, 40, and 50 mA·cm^{-2} were used to discuss the impact of charge transfer. Different initial pH values (2.0, 7.0, and 11.0) of dye solution were obtained by adding an appropriate amount of NaOH or H_2SO_4. Different temperatures (0, 10, 15, and 20℃) of electrolytes were employed to investigate the effect of temperature on degradation efficiency, which was controlled by the constant temperature water-bathing. Moreover, effect of chloride ions was also discussed to explore the degradation efficiency of the dye. During experiments, samples were taken out from the cell every 10 min for UV-Vis measurement (Agilent 8453).The maximum adsorption wavelength of ARG is 505 nm and the colour removal efficiency of ARG was calculated as follows:

$$\text{Colour removal efficiency}\ (\%) = \frac{ABS_0 - ABS_t}{ABS_0} \times 100 \quad (1)$$

where ABS_0 and ABS_t are the absorbance values in 505 nm before electrolysis and after an electrolysis time t, respectively. The average energy consumption per gram ARG (EC_P, kWh·gARG^{-1}) was calculated according to equation (2):

$$EC_p = \frac{5}{18} \times \frac{U_{cell} \times I \times t}{C_0 \times V \times \eta} \quad (2)$$

where I is the current during reaction (A); U_{cell} is the average cell voltage (V); t is the electrolysis time (s); V is the volume of treated solution (mL); C_0 is the initial dye concentration of ARG (mg·L^{-1}); η is the removal efficiency of ARG and 5/18 is the conversion coefficient of Joule to kWh.

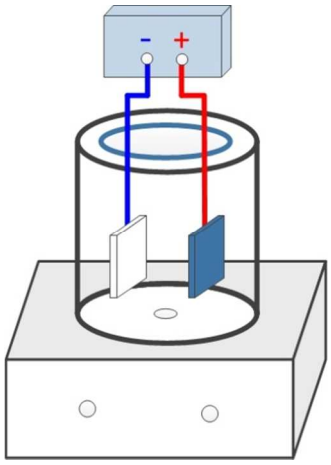

Fig.2 The sketch of electrocatalytic degradation experiment.

3. Results and discussion

3.1 Surface morphology characterization

Fig.3 shows FE-SEM of the as-prepared TiO_2 nanotube arrays electrode, Sb-SnO_2/TiO_2 nanotube arrays electrode, α-PbO_2/Sb-SnO_2/TiO_2 nanotube arrays and β-PbO_2/α-PbO_2/Sb-SnO_2/TiO_2 nanotube arrays electrode. It can be observed from Fig. 3a that there were highly ordered and uniform TiO_2 nanotube arrays grown vertically on Ti substrate, with a wall thickness of 10-15 nm and an average inner tube diameter of 115-125 nm. The cross-sectional image inset in Fig. 1a states that TiO_2 nanotube arrays were well aligned, with an average nanotube length of approximately 11 μm. We used microwave method to dope TiO_2 nanotube arrays with Sb-SnO_2, as is shown in Fig. 3b. The bottom section image of TiO_2 nanotube arrays in Fig. S1a and S1b indicate that Sb and Sn were implanted into channels of TiO_2 nanotube arrays. Moreover, it can be clearly seen that the surface is thoroughly covered by Sb-SnO_2 coating and presented a flower-like pattern. Fig. 3c displays SEM of the α-PbO_2/Sb-SnO_2/TiO_2 nanotube arrays electrode, from which we can see that the top surface is covered by many spicules. These spicules made the surface more uniform (Fig. 1Sc). After being decorated with β-PbO_2, as shown in Fig. 1Sd, a hill-like surface was observed at the macroscopic level. From microscopic perspective, the morphology of deposited PbO_2 was tetrahedron-shaped, as shown in Fig. 3d. In the visual appearance change from the acicular shape to the tetrahedron shape, a relatively homogeneous appearance and compact surface coverage were obtained. This columnar-type inset greatly increased its effective area, which was expected to result in a better electrocatalytic activity during the oxidation reaction of organic dye molecules.

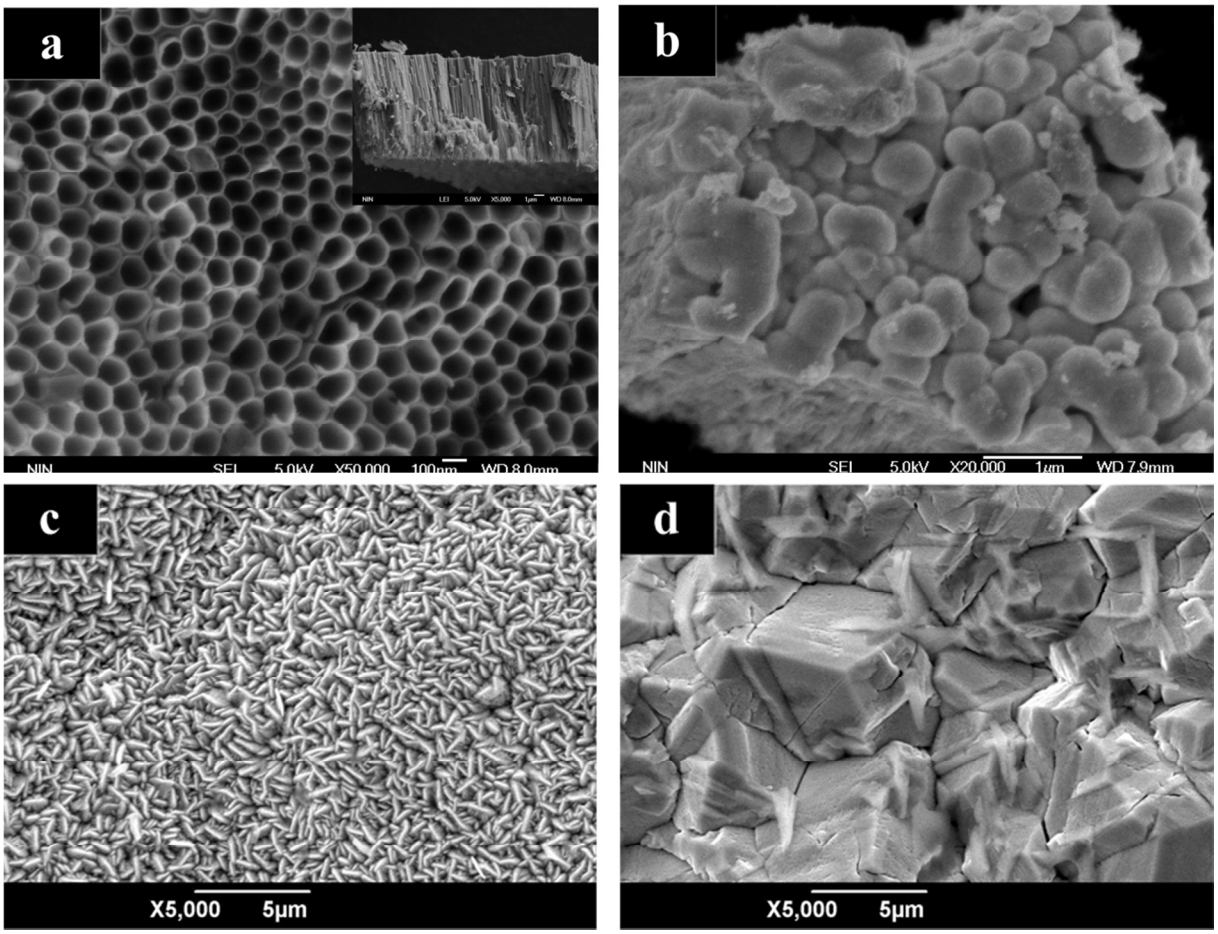

Fig. 3 FE-SEM (a) top view and cross-sectional view of plain TiO_2 NTAs; (b) top view of Sb-SnO_2/TiO_2 NTAs; (c) top view of α-PbO_2/Sb-SnO_2/TiO_2 NTAs; (d) top view of β-PbO_2/α-PbO_2/Sb-SnO_2/TiO_2 NTAs.

3.2 X-ray diffraction analysis

XRD of as-prepared TiO_2 nanotube arrays electrode, Sb-SnO_2/TiO_2 nanotube arrays electrode, α-PbO_2/Sb-SnO_2/TiO_2 nanotube arrays electrode and β-PbO_2/α-PbO_2/Sb-SnO_2/TiO_2 nanotube arrays electrode is shown in Fig. 4. It was found that bare TiO_2 nanotube arrays exhibited the reflections of anatase TiO_2. After embed with Sb-SnO_2, Sb-SnO_2/TiO_2 nanotube arrays electrode displays the characteristic reflections of SnO_2 cassiterite with a tetragonal structure. No peaks of Sb are observed due to the formation of a solid solution between Sn and Sb by substitution of Sn ions in cassiterite structure by Sb ions. In addition, no peaks corresponding to TiO_2 were detected, pointing out that the coating had a better coverage. When α-PbO_2 films were decorated on the surface of Sb-SnO_2/TiO_2 nanotube arrays electrode, there were no peaks

corresponding to SnO_2 cassiterite arising from the fact that SnO_2 interlayer was fully covered by the thick layer of α-PbO_2 film on electrode surface. In addition, XRD recorded on β-PbO_2 films deposited on α-PbO_2/Sb-SnO_2/TiO_2 nanotube arrays substrates is also shown in Fig. 4. The diffraction peaks observed at 2θ=25.4°, 32.0°, 36.2°, 49.0°, 58.9º, 60.7º, 62.5º, 74.4º are assigned to (110), (101), (200), (211), (310), (112), (301) and (321) plane of β-PbO_2. The average grain sizes of β-PbO_2 crystals calculated by Debye-Scherrer equation were 14.7 nm, which is smaller than α-PbO_2 (21.7 nm). Chen et al. [45] reported that average crystal sizes of PbO_2 by one-step electrodeposited is 29.1nm. This indicates smaller crystals sizes of PbO_2 can be obtained by the two-step electrodeposited, which means that PbO_2 is dispersed more effectively on the electrode surface. It should be noted that there were no α-PbO_2 peaks detected after deposition with β-PbO_2 due to the completely covered by β-PbO_2 coating. The results are in accordance with SEM image.

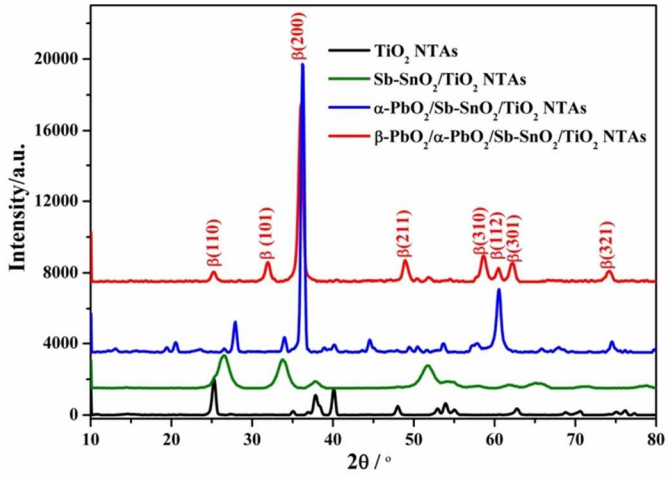

Fig. 4 XRD pattern of the different samples.

3.3 Electrochemical analysis

Fig. 5 shows linear sweep voltammetric (LSV) of the β-PbO_2/α-PbO_2/Sb-SnO_2/TiO_2 nanotube arrays electrode in the 0.5 M H_2SO_4 solution. The onset potential for oxygen evolution potential (OEP) on electrode was 1.7V (Vs.Ag/AgCl). As shown in Fig. 2S, a cathodic peak and anodic peak are appeared due to the reaction of Pb on the electrode surface. We all know that voltammetric charge (q*) of an electrode is related to its electroactive surface area. Total charge (q_T^*) and outer charge (q_o^*) are calculated by the equation (3) and the equation (4), respectively [42].

$$q^* = q_o^* + k_1 v^{-0.5} \quad (3)$$

$$q^{*-1} = q_T^{*-1} + k_2 v^{0.5} \quad (4)$$

where k_1 and k_2 are constants; v is the scan rate. Fig. 5b and Fig. 5c are the fitting of these results. It is observed that q_T^* and q_o^* was 73.5 C·cm^{-2} and 0.09 C·cm^{-2}, respectively.

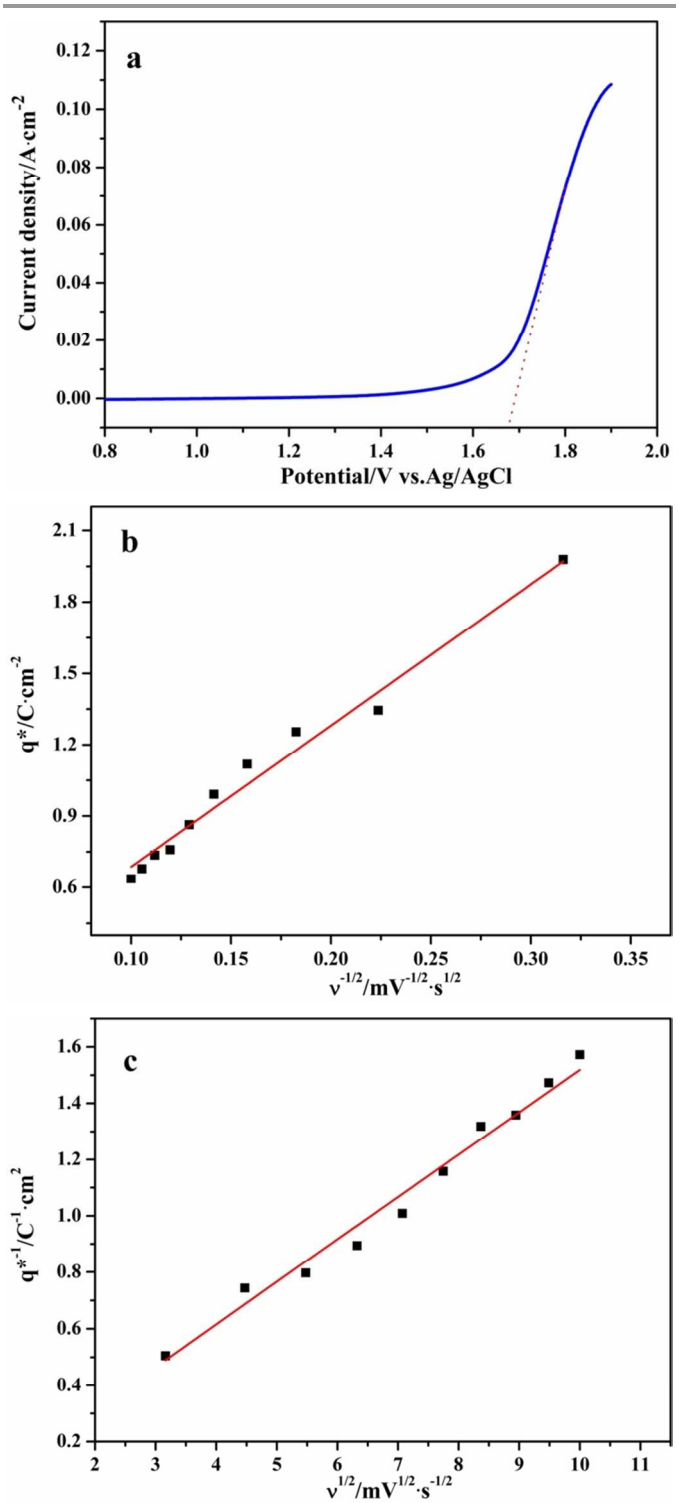

Fig. 5 (a) LSV curve for the β-PbO_2/α-PbO_2/Sb-SnO_2/TiO_2 NTAs electrode at a sacn rate of 50 mV·s^{-1}in 0.5 M H_2SO_4 solution. (b) Extrapolation of q_o^* for β-PbO_2/α-PbO_2/Sb-SnO_2/TiO_2 NTAs from the representation of q^* versus $v^{-1/2}$.(c) Extrapolation of q_T^* for β-PbO_2/α-PbO_2/Sb-SnO_2/TiO_2 NTAs from the representation of $(q^*)^{-1}$ versus $v^{1/2}$; data obtained from the cyclic voltammograms obtained between 0 and 2 V versus Ag/AgCl at various scan rates in 0.5 M H_2SO_4 solution (Fig. 2S).

EIS measurements were performed to explore charge transfer on electrode surface, as shown in Fig. 3S. The simulated circuit

consisted of solution resistance (R_s), double layer capacitance (C_{dl}), diffusion resistance (Z_w) and charge transfer resistance (R_{ct}). The change of R_{ct} could reflect the charge transfer on electrode surface. When the voltage was lower than OEP, there was no reaction on the electrode surface. If the voltage exceeded the OEP, O_2 would be generated on the electrode surface. The simulated data is shown in table. 1S, from which we found that charge transfer resistance decreased from 56.0 ohm·cm^{-2} to 20.1 ohm·cm^{-2}. This can be explained by the formation of O_2, which enhanced the charge transfer.

The accelerated life test was conducted to evaluate electrochemical stability of the β-PbO_2/α-PbO_2/Sb-SnO_2/TiO_2 nanotube arrays electrode. Fig. 6a shows the time course of cell potential in accelerated life test under 0.5 mol·L^{-1} H_2SO_4 aqueous solutions with a current density of 0.5 A·cm^{-2}. It was observed that the electrode displayed a lifetime of 815 h. Moreover, it should be noted that there existed two platforms in the curve. The first platform (4V) was attributed to the anti-corrosion of outer β-PbO_2/α-PbO_2 coating. The second platform (8.5V) arose from the formation of solid solution by β-PbO_2/α-PbO_2 and Sb-SnO_2, which made the electrode have stronger anti-corrosion.

SEM image of deactivated β-PbO_2/α-PbO_2/Sb-SnO_2/TiO_2 nanotube arrays electrode is shown in Fig. 6b and 6c. It was found that some coatings fell off from the substrate, which made the composite electrode lost its activity. Fig. 6c shows the magnified image of Fig. 6b, from which we observed that a solid solution was formed on the substrate. This phenomenon further demonstrated the formation of the second platform. EDS measurement proved that there existed two distinct regions on the electrode surface and stated the formation of the solid solution (Fig. 4S).

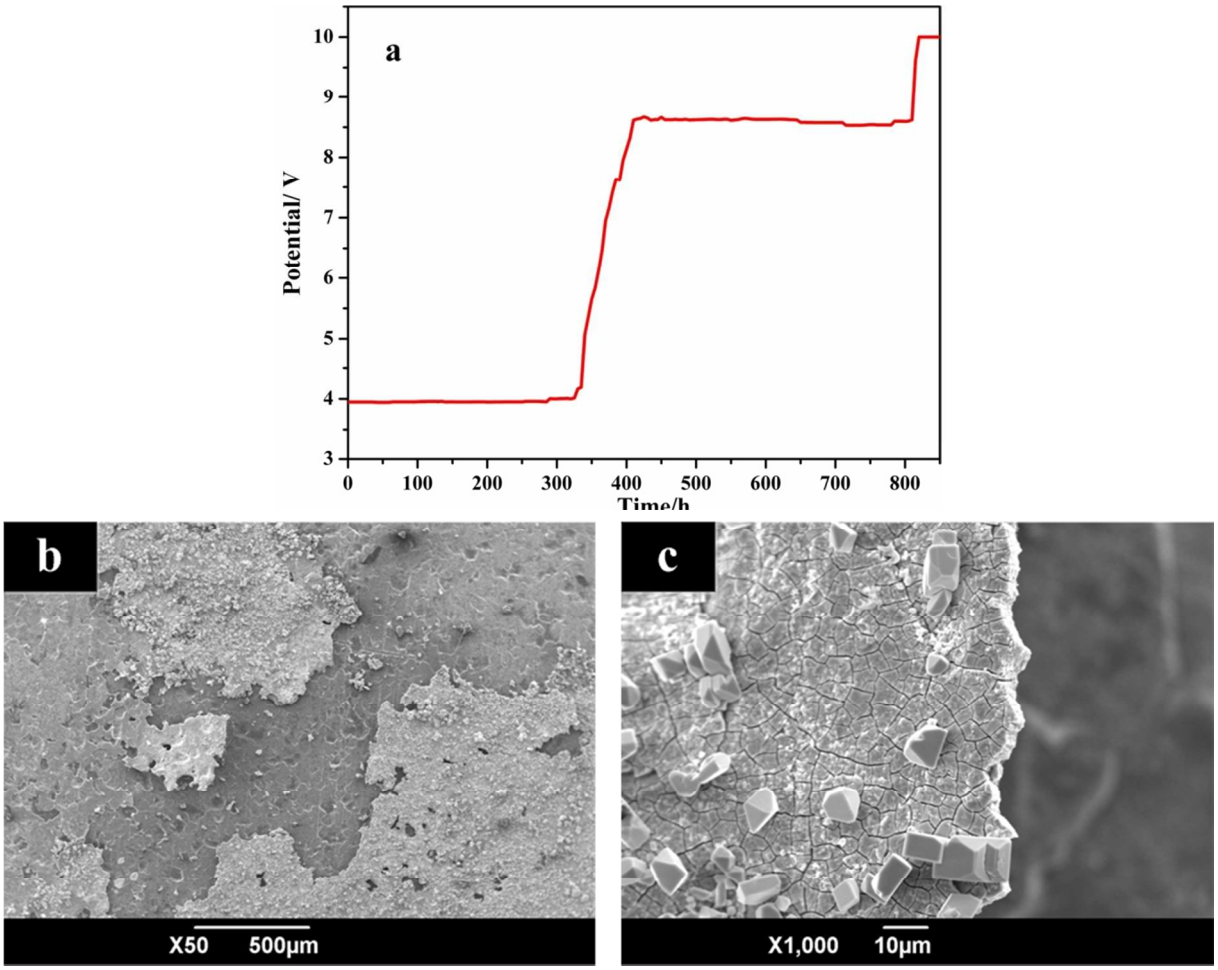

Fig. 6 (a)Variation of the cell potential with the testing time in the accelerated life test for the β-PbO_2/α-PbO_2/Sb-SnO_2/TiO_2 NTAs electrode in 0.5 M H_2SO_4 (current density: 0.5 A·cm^{-2}); FE-SEM (b) top view of the deactiviated β-PbO_2/α-PbO_2/Sb-SnO_2/TiO_2 NTAs electrode; (c) magnified image of (b).

To investigate the charge transfer on the normal electrode and the deactivated electrode, EIS measurements were conducted in H_2SO_4 solution aqueous, as shown in Fig. 7. It can be seen that the normal β-PbO_2/α-PbO_2/Sb-SnO_2/TiO_2 nanotube arrays electrode had smaller semicircle than the deactivated electrode, indicating a fast charge transfer. In addition, simulated data showed that the charge transfer resistance increased from 20.1 ohm·cm^{-2} (normal electrode) to 122.5 ohm·cm^{-2} (deactivated electrode) (Table. 2S). These results implied that the electrode might suffer a large resistance after losing its activity, which greatly weaken its electro-catalysis.

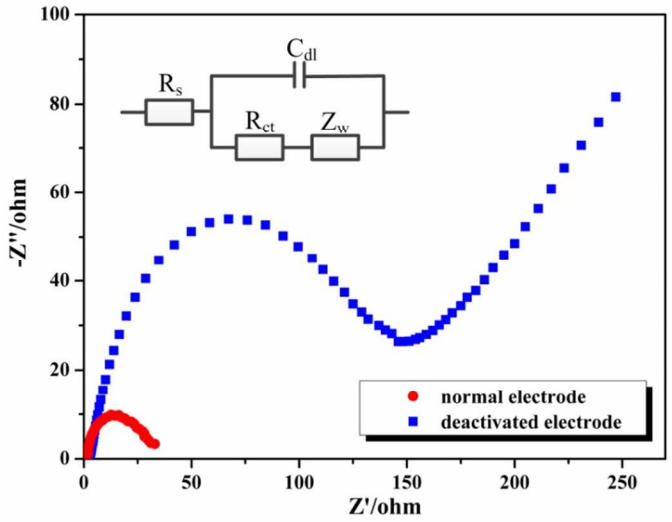

Fig. 7 EIS measurement results and the simulated circuit.

3.4 Influence of initial dye concentration and current density

Industrial wastewater often contains different concentrations of ARG, it is necessary to investigate the influence of initial dye concentration on the performance of electrocatalytic oxidation process. Fig. 8a shows that as initial dye concentration increased from 20 $mg \cdot L^{-1}$ to 100 $mg \cdot L^{-1}$, the time of total decolourization was enhanced significantly. According to literature [47], the electrocatalytic oxidation process is limited by mass transfer control. The electrochemical reaction was faster than diffusion at low concentrations and the dye could be degraded entirely on the interface. With the increase of initial concentration, hydroxyl radicals produced on electrode surface were not enough for readily degrading pollutants. Therefore, decolourization efficiency decreases with the increasing of initial concentration. We employed pseudo first-order kinetics model to simulate ARG degradation. The apparent kinetic coefficient is shown in the right corner of Fig. 8a. It is obvious that the apparent kinetic coefficient decreased with the increasing of initial concentration. This was in accordance with decolourization efficiency. Fig. 8b shows the average energy consumption per gram ARG (EC_p) of different dye concentration. It was observed that there was a positive correlation between initial dye concentration and EC_p. Moreover, the final EC_p is increased with initial dye concentration due to a long degradation time. It was also found that there were two curves overlapped in Fig. 8b due to the similar removal efficiency may reach a similar EC_p, as shown in Fig. 8a.

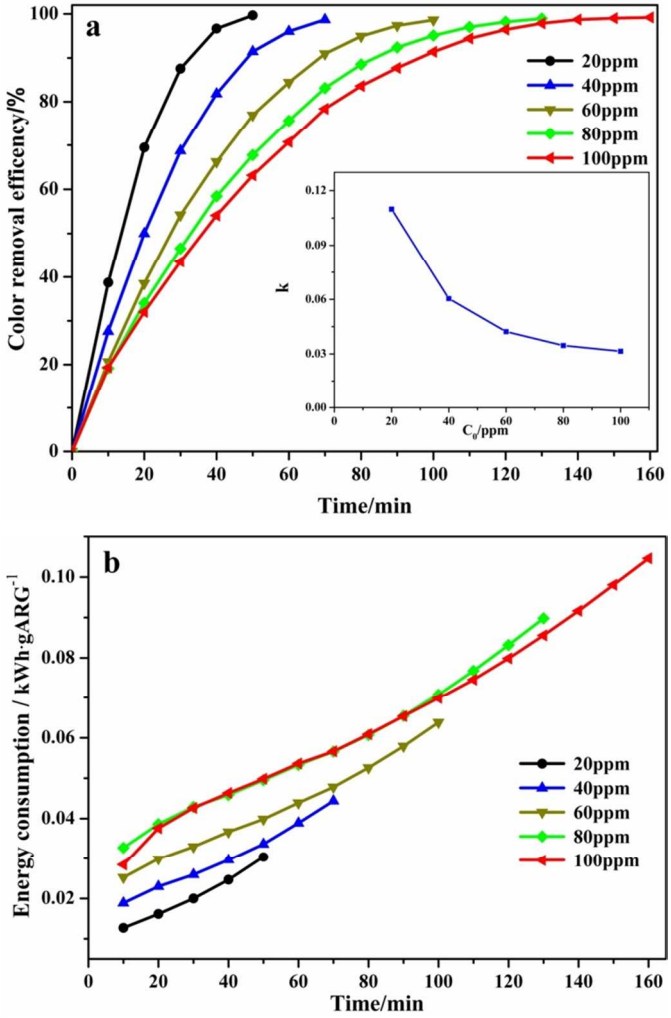

Fig. 8 Influence of initial dye concentration on the colour removal efficiency (a) and the average energy consumption per gram ARG (b). (Current density, 20 $mA \cdot cm^{-2}$; concentration of supporting electrolyte (Na_2SO_4), 0.1 M)

Fig. 9a shows the curve of colour removal efficiency with the degradation time for different current densities. Improving the current density had a positive influence on the colour removal efficiency of ARG in the range of 10-50 $mA \cdot cm^{-2}$. The reason was that a higher current density resulted in a higher generation of ·OH radicals formed in water oxidation [48, 49]. It should be pointed out that the increase of colour removal efficiency was retarded when current density was higher than 40 $mA \cdot cm^{-2}$. At low current density, ·OH radicals were not enough, the colour removal efficiency increased with the current density. At high current density, though there were excessive ·OH radicals, organic matter primarily reacted with the adsorbed ·OH radicals on the electrode surface. The mass transfer of contaminants from bulk solution to electrode surface probably became the limiting procedure. Therefore, further increasing of the current density had little influence on removal efficiency. From the value of apparent kinetic coefficient in the right corner of Fig. 9a, we can conclude that higher current density was beneficial for the electrocatalytic oxidation process. Fig. 9b shows the average energy consumption per gram ARG (EC_p) of various

current densities. As shown in Fig. 9b, we found that higher current density resulted in a larger EC_p. In other words, current density had a positive impact on the energy consumption per gram ARG. Considering the EC_p, exceeding current density is not rational in practical industry. Fig. 10 is the digital image of decolourization at the current density of 50 $mA \cdot cm^{-2}$ for different degradation time. It is clear to see the change of decolourization. Hence, we concluded that the current densities played a significant role in the electrocatalytic oxidation process.

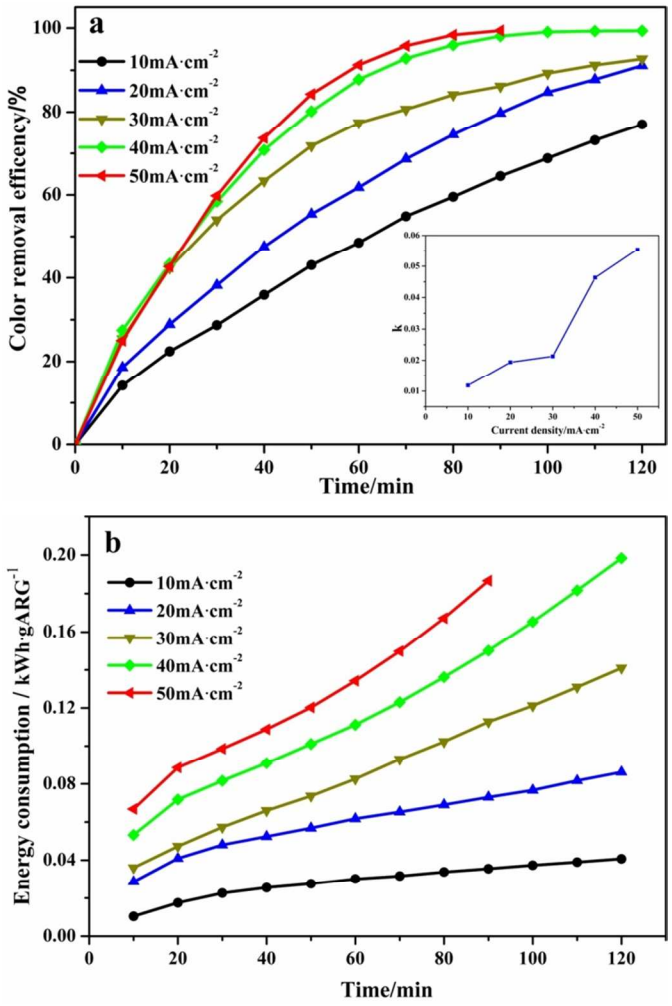

Fig. 9 Influence of the current density on the colour removal efficiency (a) and the average energy consumption per gram ARG (b). (Initial dye concentration of ARG, 100 $mg \cdot L^{-1}$; concentration of supporting electrolyte (Na_2SO_4), 0.1 M)

Fig. 10 The digital image of decolourization. (Initial dye concentration of ARG, 100 $mg \cdot L^{-1}$; current density, 50 $mA \cdot cm^{-2}$; concentration of supporting electrolyte (Na_2SO_4), 0.1 M)

3.5 Influence of initial pH, temperature of electrolyte and chloride ions

Initial pH can impact the morphology of coexisting ions or organic matter. Hence, the effect of initial pH was investigated to obtain more extensive application prospect in practical wastewater. Fig. 11a shows the curve of colour removal efficiency with the degradation time for different initial pH. It was obvious that the ultimate colour removal efficiency had little distinction. From the value of apparent kinetic coefficient in the right corner of Fig. 11a, we obtained similar results. However, there exists a significant distinction at the beginning of degradation time. The alkaline conditions had the higher colour removal efficiency than neutral and acidic conditions. The possible explanation was that more ·OH radicals were formed in alkaline conditions, which caused a remarkable improvement of colour removal efficiency at the beginning of the degradation time [48]. Fig. 11b exhibits the average energy consumption per gram ARG (EC_p) of different initial pH. It was found that neutral condition had the smallest EC_p among these three conditions. Hence, pH adjustment was not necessary in the processing for the degradation of ARG, and the electro-catalysis could work well in a wide pH range.

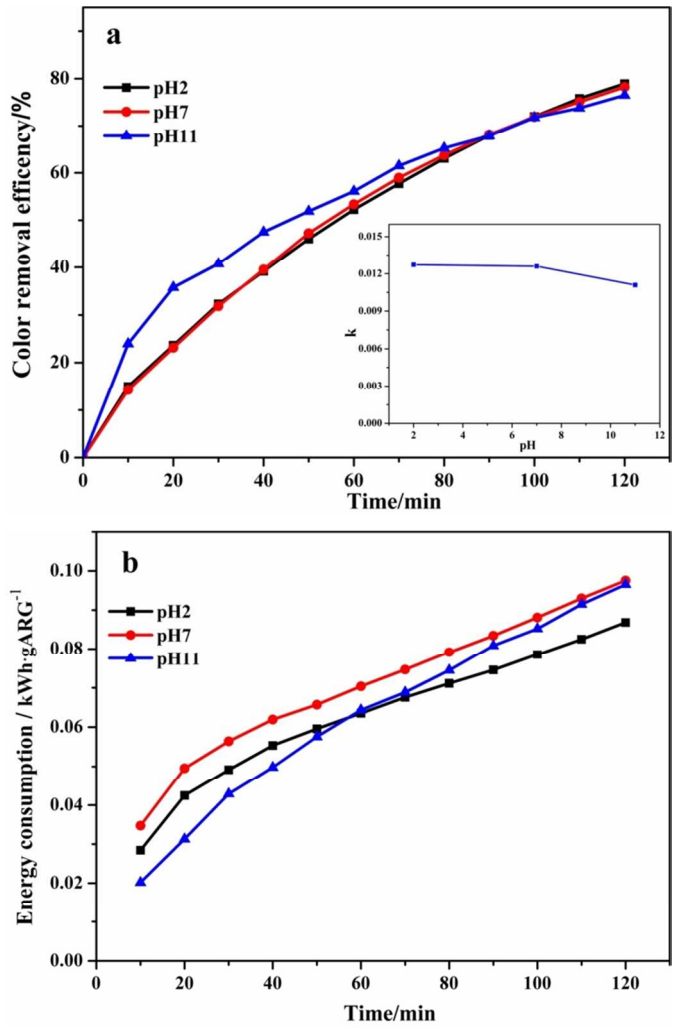

Fig. 11 Influence of initial pH on the colour removal efficiency (a) and unit energy consumption (b). (Initial dye concentration of ARG, 100 mg·L^{-1}; current density, 20 mA·cm^{-2}; concentration of supporting electrolyte (Na_2SO_4), 0.1 M)

Most of reactions are related to the temperature, thus it is necessary to investigate influence of temperature. We employed the constant temperature bath to control the temperature of electrolyte. As shown in Fig. 12a, temperature had little effects on electrocatalytic oxidation between 0 ℃ and 20 ℃. The possible reason was that low temperature could not significantly affect the amount of ·OH radicals which were absorbed on the electrode surface. However, the specific mechanism was not clear, so further study was needed. Fig. 12b shows the average energy consumption per gram ARG (EC_p) of different temperatures. It was found that temperature had a negative influence on EC_p. Meanwhile, the increase of temperature needs to consume the extra heat. Thus, whether the adjustment of temperature was worthy for dye wastewater treatment should be carefully weighed.

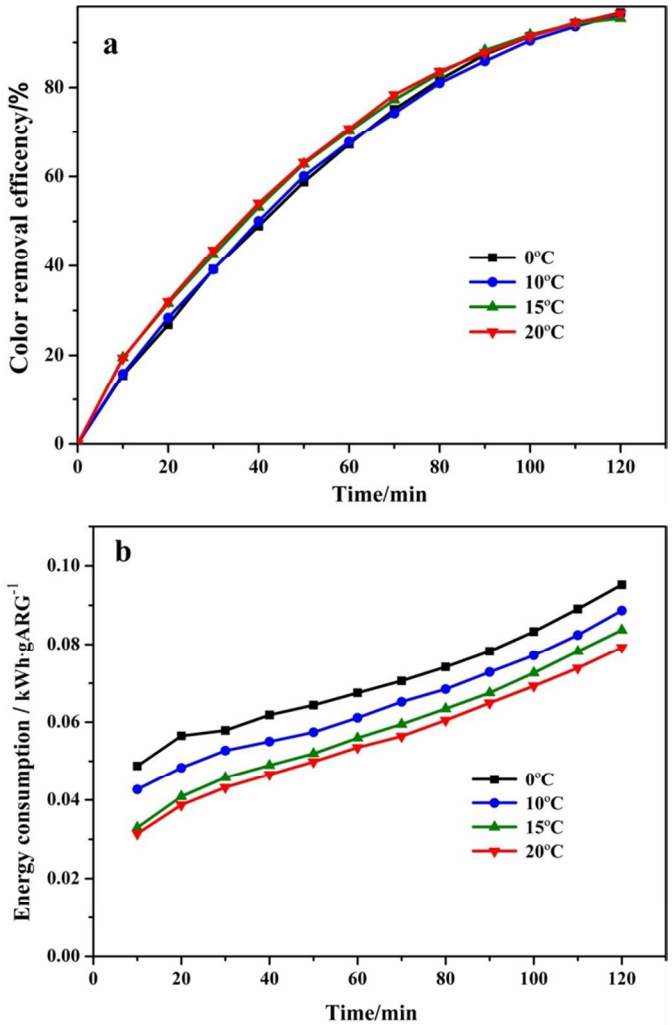

Fig. 12 Influence of temperature on the colour removal efficiency (a) and unit energy consumption (b). (Initial dye concentration of ARG, 100 mg·L^{-1}; current density, 20 mA·cm^{-2}; concentration of supporting electrolyte (Na_2SO_4), 0.1 M)

As we all known, wastewater from print industry and textile industry often contains chloride ions, thus the influence of chloride ions on the colour removal efficiency should be discussed. Fig. 13 reveals that chloride ions have a significant positive effect on the colour removal efficiency for many active chlorine species can be generated via direct oxidation of chloride ions on the electrode surface [50]. Because of the high oxidation performance of the active chlorine, there was a significant difference in the colour removal efficiency. Other researchers have obtained similar conclusions [43]. Fig. 13b shows the average energy consumption per gram ARG (EC_p) of two conditions, from which we found that the addition of chloride ions was greatly decreased EC_p. However, the cost of potential pollution should be considered. Hence, whether to add the chloride ions to dye wastewater treatment is still a problem which should be carefully weighed.

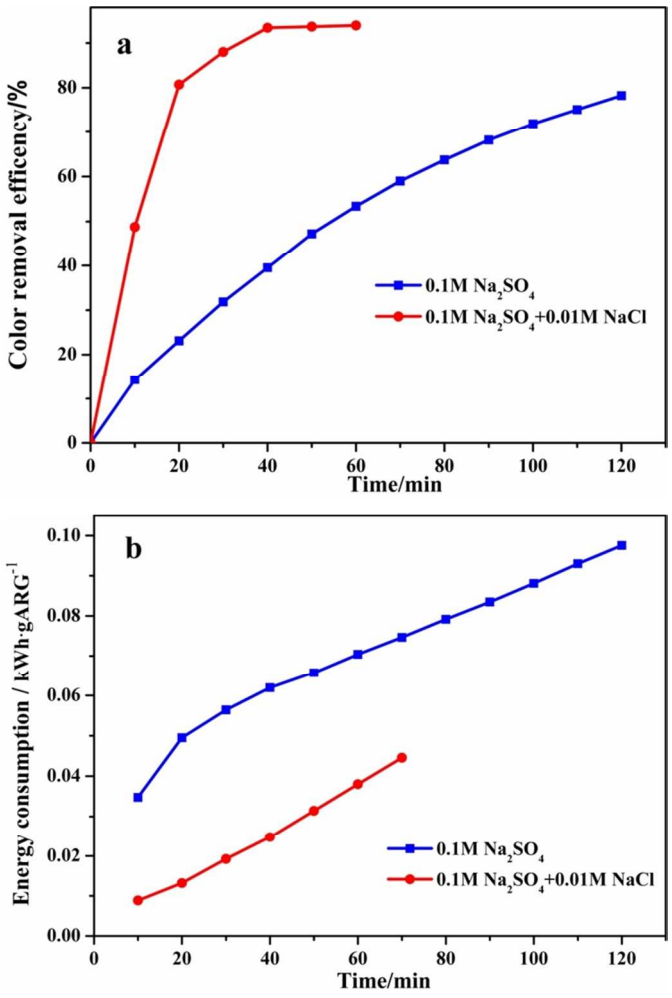

Fig. 13 Influence of the chloride on the colour removal efficiency (a) and unit energy consumption (b). (Initial dye concentration of ARG, 100 mg·L^{-1}; current density, 20 mA·cm^{-2}; concentration of supporting electrolyte (Na_2SO_4), 0.1 M)

3.6 UV-Vis analysis of the degradation process

UV-Vis absorbance spectrum of the ARG degradation process is shown in Fig. 14. It was learned from Fig. 14 that ARG consisted of benzene ring, naphthalene ring, and azo group. As

the electrochemical degradation proceeded, benzene ring and naphthalene ring disappeared successively due to the free radical attack and then decomposed to form some small organic molecules [43]. Meanwhile, it could be found that azo group in the dye molecule was worn off within 80 min, indicating the destruction of –N=N- group. However, further studies regarding the specific degradation mechanism in the electrocatalytic oxidization are required and relevant research work is under investigation.

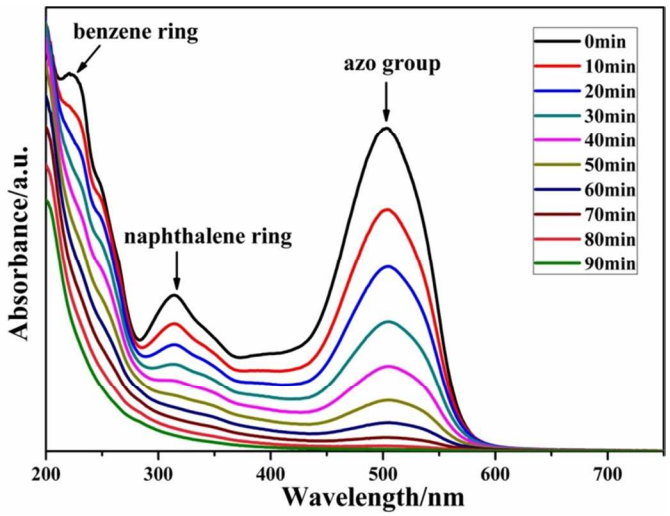

Fig. 14 UV-Vis absorbance spectrum of the degradation process.(Initial dye concentration of ARG, 100 mg·L^{-1}; current density, 50 mA·cm^{-2}; concentration of supporting electrolyte (Na_2SO_4), 0.1 M)

4. Conclusion

A novel β-PbO_2/α-PbO_2/Sb-SnO_2/TiO_2 nanotube arrays electrode was fabricated by combining the microwave and electrodepositon method. The composite electrode has an ordered multilayer structure with TiO_2 nanotube arrays as a tubal template and Sb-SnO_2 coating as an interlayer. This special microstructure exhibited an enhanced electrocatalytic activity and a high oxygen evolution reaction potential (1.7 V). In addition, the ordered multilayer structure significantly improved the service lifetime (815 h) of the composite electrode. Acid Red G (ARG) was employed as a model organic pollutant for electrochemical degradation to evaluate its electrocatalytic activity. Several operation variables, such as initial concentration, current densities, initial pH values, temperature of electrolyte and chloride ions were investigated to explore the removal efficiency of ARG. It was found that initial concentration, chloride ions and current densities could significantly affect the colour removal efficiency. However, initial pH values and temperature of electrolyte had little influence on colour removal efficiency. It is known that the addition of chloride ions can largely improve the colour removal efficiency, but whether it is worthy to add chloride ions should be carefully weighed. In summary, the novel β-PbO_2/α-PbO_2/Sb-SnO_2/TiO_2 nanotube arrays electrode exhibited an enhanced electrocatalytic activity and electrochemical stability. Further studies on exploring the composite electrode will be conducted in the future.

Acknowledgments

The authors gratefully acknowledge the financial supports from the National Natural Science Foundation of China (Grant No. 21307098), China Postdoctoral Science Foundation （2013M532053）and the Fundamental Research Funds for the Central Universities of China.

Notes and references

[a]Department of Environmental Science and Engineering, Xi'an Jiaotong University, Xi'an 710049, China
[b]State Key Laboratory of Multiphase Flow in Power Engineering, Xi'an Jiaotong University, Xi'an 710049, China
Corresponding authors:
E-mail: xuhao@mail.xjtu.edu.cn; yanwei@mail.xjtu.edu.cn
Tel.: +86-13032912105; fax: +86-29-82664731.

1. C. A. Martinez-Huitle, S. Ferro and A. De Battisti, *Electrochim. Acta*, 2004, **49**, 4027-4034.
2. G. H. Chen, *Sep. Purif. Technol.*, 2004, **38**, 11-41.
3. C. A. Martinez-Huitle and E. Brillas, *Appl. Catal. B*, 2009, **87**, 105-145.
4. W. Wu, Z.-H. Huang and T.-T. Lim, *Appl. Catal. A*, 2014, **480**, 58-78.
5. D. Valero, V. García-García, E. Expósito, A. Aldaz and V. Montiel, *Sep. Purif. Technol.*, 2014, **123**, 15-22.
6. P. S. Patel, N. Bandre, A. Saraf and J. P. Ruparelia, *Procedia Eng.*, 2013, **51**, 430-435.
7. M. Panizza, P. A. Michaud, G. Cerisola and C. Comninellis, *Electrochem. Commun.*, 2001, **3**, 336-339.
8. B. Marselli, J. Garcia-Gomez, P. A. Michaud, M. A. Rodrigo and C. Comninellis, *J. Electrochem. Soc.*, 2003, **150**, D79-D83.
9. X. Zhu, J. Ni and P. Lai, *Water Res.*, 2009, **43**, 4347-4355.
10. L. Marincic and F. B. Leitz, *J. Appl. Electrochem.*, 1978, **8**, 333-345.
11. C. Bock and B. MacDougall, *J. Electroanal. Chem.*, 2000, **491**, 48-54.
12. C. P. De Pauli and S. Trasatti, *J. Electroanal. Chem.*, 2002, **538–539**, 145-151.
13. K. W. Kim, E. H. Lee, J. S. Kim, K. H. Shin and B. I. Jung, *J. Electrochem. Soc.*, 2002, **149**, D187-D192.
14. P. Duverneuil, F. Maury, N. Pebere, F. Senocq and H. Vergnes, *Surf. Coat. Technol.*, 2002, **151–152**, 9-13.
15. A. C. Chen and S. Nigro, *J. Phys. Chem. B*, 2003, **107**, 13341-13348.
16. X. Chen and G. Chen, *Electrochim. Acta*, 2005, **50**, 4155-4159.
17. B. Wang, W. Kong and H. Ma, *J. Hazard. Mater.*, 2007, **146**, 295-301.
18. H. Xu, C. L. Tang, Q. Zhang and W. Yan, *J. Inorg. Mater.*, 2012, **27**, 667-671.
19. L. Zhang, L. Xu, J. He and J. Zhang, *Electrochim. Acta*, 2014, **117**, 192-201.
20. B. Xue, Y. Zhang and J. Y. Wang, *Procedia Environ. Sci.*, 2011, **10**, Part A, 647-652.
21. X. Li, X. Li, S. Tang, J. Yang, W. Li, B. Luo, Y. Yu and S. Li, *Appl. Surf. Sci.*, 2014, **311**, 357-361.

22. Q. Dai, Y. Xia, C. Sun, M. Weng, J. Chen, J. Wang and J. Chen, *Chem. Eng. J.*, 2014, **245**, 359-366.
23. A. Mukimin, H. Vistanty and N. Zen, *Chem. Eng. J.*, 2015, **259**, 430-437.
24. J. F. Niu, H. Lin, J. L. Xu, H. Wu and Y. Y. Li, *Environ. Sci. Technol.*, 2012, **46**, 10191-10198.
25. H. Lin, J. F. Niu, J. L. Xu, H. O. Huang, D. Li, Z. H. Yue and C. H. Feng, *Environ. Sci. Technol.*, 2013, **47**, 13039-13046.
26. H. Lin, J. Niu, J. F. Xu, Y. Li and Y. Pan, *Electrochim. Acta*, 2013, **97**, 167-174.
27. H. Lin, J. F. Niu, S. Ding and L. Zhang, *Water Res.*, 2012, **46**, 2281-2289.
28. P. Yao, *Desalination*, 2011, **267**, 170-174.
29. B. CorreaLozano, C. Comninellis and A. DeBattisti, *J. Appl. Electrochem.*, 1997, **27**, 970-974.
30. Q. Chen, S. Ai, S. Li, J. Xu, H. Yin and Q. Ma, *Electrochem. Commun.*, 2009, **11**, 2233-2236.
31. C. Ma, F. Tan, H. Zhao, S. Chen and X. Quan, *Sens. Actuators B*, 2011, **155**, 114-119.
32. W. Han, Y. Chen, L. Wang, X. Sun and J. Li, *Desalination*, 2011, **276**, 82-88.
33. H. An, Q. Li, D. Tao, H. Cui, X. Xu, L. Ding, L. Sun and J. Zhai, *Appl. Surf. Sci.*, 2011, **258**, 218-224.
34. H. Liu, S. Yu, T. Shen, S. Tong and C. Ma, *Sep. Purif. Technol.*, 2014, **132**, 27-32.
35. J. Zhao, C. Zhu, J. Lu, C. Hu, S. Peng and T. Chen, *Electrochim. Acta*, 2014, **118**, 169-175.
36. X. Duan, Y. Zhao, W. Liu, L. Chang and X. Li, *J. Taiwan Inst. Chem. Eng.*, 2014, **45**, 2975-2985.
37. L. Chang, Y. Zhou, X. Duan, W. Liu and D. Xu, *J. Taiwan Inst. Chem. Eng.*, 2014, **45**, 1338-1346.
38. L. S. Andrade, L. A. M. Ruotolo, R. C. Rocha-Filho, N. Bocchi, S. R. Biaggio, J. Iniesta, V. García-Garcia and V. Montiel, *Chemosphere*, 2007, **66**, 2035-2043.
39. J. Cao, H. Zhao, F. Cao, J. Zhang and C. Cao, *Electrochim. Acta*, 2009, **54**, 2595-2602.
40. H. Xu, D. Shao, Q. Zhang, H. H. Yang and Y. Wei, *Rsc Advances*, 2014, **4**, 25011-25017.
41. X. Cui, G. H. Zhao, Y. Z. Lei, H. X. Li, P. Q. Li and M. C. Liu, *Mater. Chem. Phys.*, 2009, **113**, 314-321.
42. Y. Chen, L. Hong, H. Xue, W. Han, L. Wang, X. Sun and J. Li, *J. Electroanal. Chem.*, 2010, **648**, 119-127.
43. H. An, H. Cui, W. Zhang, J. Zhai, Y. Qian, X. Xie and Q. Li, *Chem. Eng. J.*, 2012, **209**, 86-93.
44. Q. Wang, T. Jin, Z. Hu, L. Zhou and M. Zhou, *Sep. Purif. Technol.*, 2013, **102**, 180-186.
45. Y. Chen, H. Li, W. Liu, Y. Tu, Y. Zhang, W. Han and L. Wang, *Chemosphere*, 2014, **113**, 48-55.
46. W. Han, C. Zhong, L. Liang, Y. Sun, Y. Guan, L. Wang, X. Sun and J. Li, *Electrochim. Acta*, 2014, **130**, 179-186.
47. C. A. Martinez-Huitle and S. Ferro, *Chem. Soc. Rev.*, 2006, **35**, 1324-1340.
48. M. H. Miles, G. Kissel, P. W. T. Lu and S. Srinivasan, *J. Electrochem. Soc.*, 1976, **123**, 332-336.
49. D. Reyter, D. Belanger and L. Roue, *Water Res.*, 2010, **44**, 1918-1926.
50. D. Rajkumar, B. J. Song and J. G. Kim, *Dyes Pigments*, 2007, **72**, 1-7.